DOT/FAA/AR-06/37

Office of Aviation Research and Development
Washington, DC 20591

Analysis of Residual Strength of Flat and Curved Panels, With and Without Stiffeners, With Multiple-Site Damage

December 2006

Final Report

U.S. Department of Transportation
Federal Aviation Administration

NOTICE

Technical Report Documentation Page

1. Report No.	2. Government Accession No.	3. Recipient's Catalog No.
DOT/FAA/AR-06/37		

4. Title and Subtitle	5. Report Date
ANALYSIS OF RESIDUAL STRENGTH OF FLAT AND CURVED PANELS, WITH AND WITHOUT STIFFENERS, WITH MULTIPLE-SITE DAMAGE	December 2006
	6. Performing Organization Code

7. Author(s)	8. Performing Organization Report No.
M.F.J. Koolloos, F.P. Grooteman, and H.J. ten Hoeve	

9. Performing Organization Name and Address	10. Work Unit No. (TRAIS)
National Aerospace Laboratory NRL	
	11. Contract or Grant No.

12. Sponsoring Agency Name and Address	13. Type of Report and Period Covered
U.S. Department of Transportation Federal Aviation Administration Office of Aviation Research and Development Washington, DC 20591	Final Report
	14. Sponsoring Agency Code

15. Supplementary Notes

The Federal Aviation Administration Airport and Aircraft Safety R&D Division Technical Monitor was Felix Abali.

16. Abstract

Multiple-site damage (MSD) is a typical problem for aging aircraft. The large number of fuselage pressurization cycles may cause fatigue cracking at multiple rivet locations in the lap joints of an aircraft structure and thereby reduce the overall structural integrity.

The residual strength of a panel with a leading crack and MSD cracks is known to be lower than the one for a panel with the same leading crack but without MSD. A lot of research in testing and development of models have been conducted in recent years to assess the residual strength and predict linkup of stiffened flat panels with a leading crack and MSD. But differences exist between the models in terms of definitions and criteria used for crack growth and linkup, and model verification was done with experimental data available from public literature and not from direct experiments. The main objective of this project was to develop an engineering tool that can be used in the design of aircraft.

In this research project, a model to predict linkup and residual strength in flat and curved panels with a leading crack and MSD cracks and with or without stiffeners was developed. The model uses the strip yield model (as implemented in the NASGRO software), J-integral, and the compatibility methods. The strip yield method was used to calculate the stresses and deformations at the crack tips. These stresses and deformations were then used in the calculations of the J-integral values at the crack tips. The effect of the stiffeners on the deformation behavior of the panels was implemented by the displacement compatibility method, whereas the panel curvature was modelled using bulging factors.

Finally, the model was verified with experimental data obtained from testing the flat and curved panels with or without stiffeners.

17. Key Words	18. Distribution Statement
Widespread fatigue damage, Multiple-site damage, Stress intensity factor, Crack tip opening displacement, J-integral, Residual strength, Fracture mechanics, Flow stress, Crack driving force, R-curve, Strain energy release rate	This document is available to the public through the National Technical Information Service (NTIS) Springfield, Virginia 22161.

19. Security Classif. (of this report)	20. Security Classif. (of this page)	21. No. of Pages	22. Price
Unclassified	Unclassified	35	

TABLE OF CONTENTS

LIST OF FIGURES

LIST OF TABLES

LIST OF ACRONYMS AND SYMBOLS

σ_R	Stress remote from crack
σ_Y	Flow stress
G	Crack driving force (strain energy release rate)
lig1	Tip-to-tip distance between leading crack and first MSD crack
lig2	Tip-to-tip distance between MSD cracks
v	Displacements in y direction
ASTM	American Society of Testing and Material
COD	Crack opening displacement
CTOD	Crack tip opening displacement
MSD	Multiple-site damage
NIST	National Institute of Standards and Technology
UTS	Ultimate tensile strength

EXECUTIVE SUMMARY

Multiple-site damage (MSD) is a typical problem for aging civil and transport aircraft, where large numbers of fuselage pressure cycles may cause fatigue cracking at multiple rivet locations. The residual strength of a panel with a leading crack and MSD cracks is lower than that of a panel with the same leading crack but without MSD. This report presents an advanced engineering model developed by the National Aerospace Laboratory to predict linkup and residual strength in flat and curved panels with one leading crack and MSD cracks, with or without stiffeners. The model was verified with experimental data published in the open literature from three different institutes. The predicted linkup loads and residual strengths correlated fairly well with the experimental values. The observed deviations for the linkup stresses fell within the experimental errors reported in the literature. The *R*-curve approach in combination with actual crack impingement as linkup criterion resulted in good predictions for the linkup stresses and the crack growth during the linkup phase. However, the predictions for residual strength and crack growth just before failure were generally higher than the measured values, owing to unreliability of the *R*-curve for long cracks. The chosen bulging factor seemed to account well for the bulging effect due to panel curvature.

1. INTRODUCTION.

The Aloha Airlines accident in 1988 (see figure 1) focused attention on the multiple-site damage (MSD) phenomenon of riveted lap joints in aircraft fuselages. MSD is a typical problem for aging aircraft, where large numbers of fuselage pressure cycles may cause fatigue cracking at multiple rivet locations in lap joints. After some growth of the MSD cracks, they may interact and crack linkup may occur, resulting in one leading crack flanked by MSD cracks [1 and 2].

FIGURE 1. PICTURE GALLERY OF THE ALOHA AIRLINES FLIGHT 243 ACCIDENT ON APRIL 28, 1988
(The aircraft suffered separation of the top of the fuselage while cruising at 24,000 feet, resulting in explosive decompression and severe structural damage. One flight attendant was sucked out of an opening in the fuselage. The plane subsequently made a safe emergency landing.)

MSD reduces overall structural integrity. Consequently, the residual strength of a panel with a leading crack and MSD cracks is known to be lower than that of a panel with the same leading crack but without MSD [2]. In recent years, research projects have been carried out to assess the residual strength of flat, stiffened panels with a leading crack and MSD cracks. Tests were conducted on flat panels (stiffened and unstiffened) with a leading crack and MSD cracks [3 through 7], and models were developed to predict linkup of the MSD cracks and the residual strength of a panel with MSD [5 through 8]. The main differences between the models arise from the definitions and criteria for crack growth and linkup. Verification of the models was done with experimental data available from publicly available literature. At the National Aerospace Laboratory (NLR), a model to predict linkup and the residual strength in both flat unstiffened and stiffened panels in the presence of MSD has been developed. The main objective was to develop an engineering tool that can be used in the design of aircraft. The model was based on the Strip Yield model (as implemented in the NASGRO software) for the calculation of the value of the *J*-integral at all crack tips and was also based on the *R*-curve approach. The influence of stiffeners was modeled using the displacement compatibility method, and the effect of panel curvature was modeled using a bulging factor.

This report presents the NLR model and its verification in the following order: (1) the Strip Yield model, (2) the residual strength model, (3) description of the displacement compatibility method and the bulging factor, and (4) verification of the model based on experimental available data.

2. STRIP YIELD MODEL.

2.1 MODEL DESCRIPTION.

The Strip Yield model uses a method first proposed by Dugdale [9] to calculate the stresses and deformations around a loaded crack by considering the material to act as a series of elements behaving in a rigid plastic manner. For a thin strip lying along, but larger in size, the fictitious crack length (i.e., the actual crack and the plastic zone ahead of the crack tip), the following conditions are assumed:

- All plastic deformation is confined within an infinitely thin strip located along the crack line.
- Material within the strip behaves in a rigid plastic manner, while material outside the strip is perfectly elastic.
- The material in the strip is able to undergo an arbitrary stretch in the tensile direction when the stress exceeds the local yield stress, both in tension and compression.

The Strip Yield model uses numerical methods to solve for stresses and deformations. The crack and the plastic zone ahead of it are divided into a number of finite width elements. Each element carries a constant stress across its width or a point force acting at its center (depending on the method used to calculate the influence functions).

An element in the plastic zone can carry a stress up to the local yield limit in tension or compression. Elements on the crack surface can carry compressive stresses up to the local yield limit. The displacements of all elements are determined from the remote load σ_R and the element stresses $\sigma(x)$, see figure 2. The basic solutions for these displacements are obtained from the Westergaard solutions [10] for the two loading conditions, yielding the following expression for the total displacement at element i:

$$v(i) = v_s(i)\sigma_R + GM(i, j)\sigma(j) \tag{1}$$

where v_s and GM are the coefficient vector and matrix for the remote load and crack surface load, respectively, and $\sigma(j)$ is the stress in element j. It must be noted that for the present model, GM can be solved for panels of infinite and finite width.

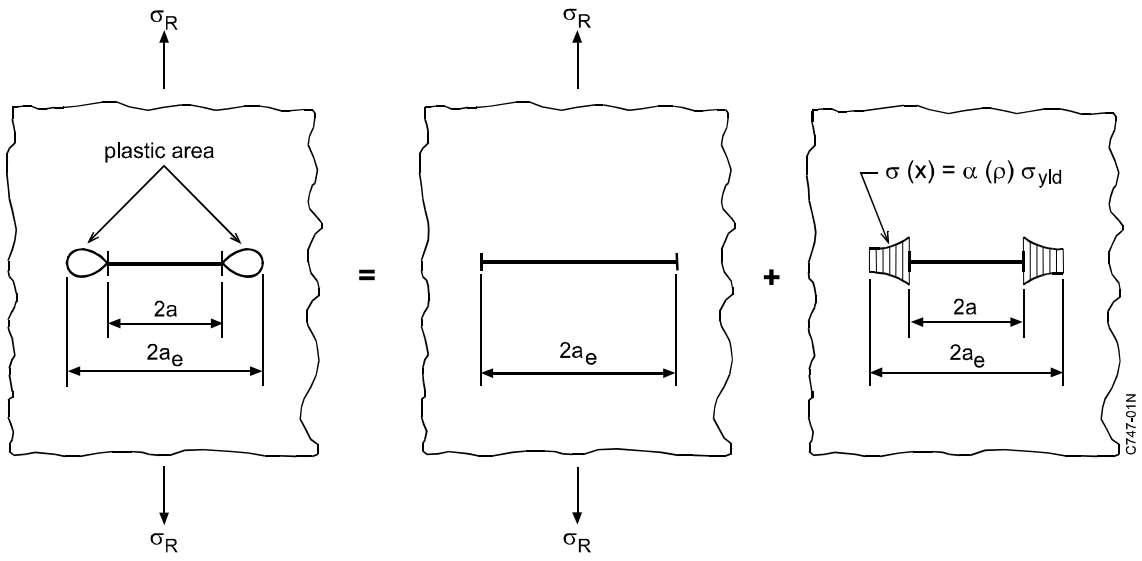

FIGURE 2. THE FICTITIOUS CRACK LENGTH ($2a_e$) AND LOAD CASES USED IN THE STRIP YIELD MODEL

The deformations in the plastic area ahead of the crack tip are determined as follows. Since the material behaves in a rigid plastic manner, elements loaded to the yield limit can undergo an arbitrary stretch, referred to as *sl*. The stretch of these elements is dictated by the elastic surrounding of the plastic area. Consider a point in the elastic area just above an element that is yielding in tension as the result of a remote load. This point is connected to the mid-plane (plane of the crack) via the yielding element and is displaced over a distance $v(i)$, see equation 1. The crack opening displacement (COD) of all elements in the plastic zone is zero. In other words, the conditions for the plastic zone are

$$sl(i) = v(i) \tag{2}$$

$$COD(i) = 0 \tag{3}$$

In the cracked area, the COD is equal to the calculated $v(i)$ minus the stretch left in the element, resulting from the loads applied to the structure when the element was part of the plastic zone:

$$COD(i) = v(i) - sl(i) \tag{4}$$

If the calculated $v(i)$ is less than the stretch left in the element, the crack is closed. The stretch is set to $v(i)$ and, hence, the COD is set to zero, as shown in equations 5 and 6.

$$sl(i) = v(i) \tag{5}$$

$$COD(i) = 0 \tag{6}$$

From these equations, the element stresses, CODs, and stretches can be solved, taking into account the following stress boundary conditions.

$$\alpha_1 \sigma_{yld} \le \sigma(i) \le \alpha_2 \sigma_{yld} \tag{7}$$

$$\alpha_1 \sigma_{yld} < \sigma(i) \le 0 \tag{8}$$

in the closed part of the crack, and

$$\sigma(i) = 0 \tag{9}$$

in the open part of the crack. In these equations, σ_{yld} is the uniaxial yield limit of the material, and α_1 and α_2 are material parameters accounting for the constraint to simulate two- and three-dimensional effects in the stress field surrounding the crack tip. Equations 1 through 9 are solved iteratively using the Gauss-Seidel solution procedure.

2.2 *J*-INTEGRAL.

Since the plastic zone near a crack tip cannot be considered negligibly small, the strain energy release rate, *G*, is obtained from the *J*-integral. For the Strip Yield model, it has been shown that there exists a simple relation between the *J*-integral and the crack tip opening displacement (CTOD) [11 and 12]. The CTOD is a somewhat artificial mathematical quantity that cannot be verified experimentally. The relation between *J* and CTOD is

$$J = \sigma_{yld} \, CTOD \tag{10}$$

The stretches at the element centers are one set of quantities obtained from a solution of the Strip Yield model. The CTOD can be calculated from the stretches of the first two elements in the plastic zone (the ones just ahead of the crack tip). From this CTOD, the *J*-integral is calculated according to the relation given above.

2.3 MULTIPLE-SITE DAMAGE.

In the case of MSD, the series of collinear cracks can be modeled as the superposition of known cases, as shown in figure 3. A surface load has to be applied to the ligaments between the cracks to close the crack locally. The stresses required to fulfill this condition are bounded by the yield stress. These stresses are obtained directly from the Strip Yield model, if it is solved with the boundary conditions given in equations 5 and 6 and applied to the ligaments between the cracks and the plastic zones outside the outer crack tips. From this solution, the opening stress and the *J*-integral can be calculated for all tips. In addition, for small-scale yielding conditions, the stress-intensity factors can be calculated from the CTODs.

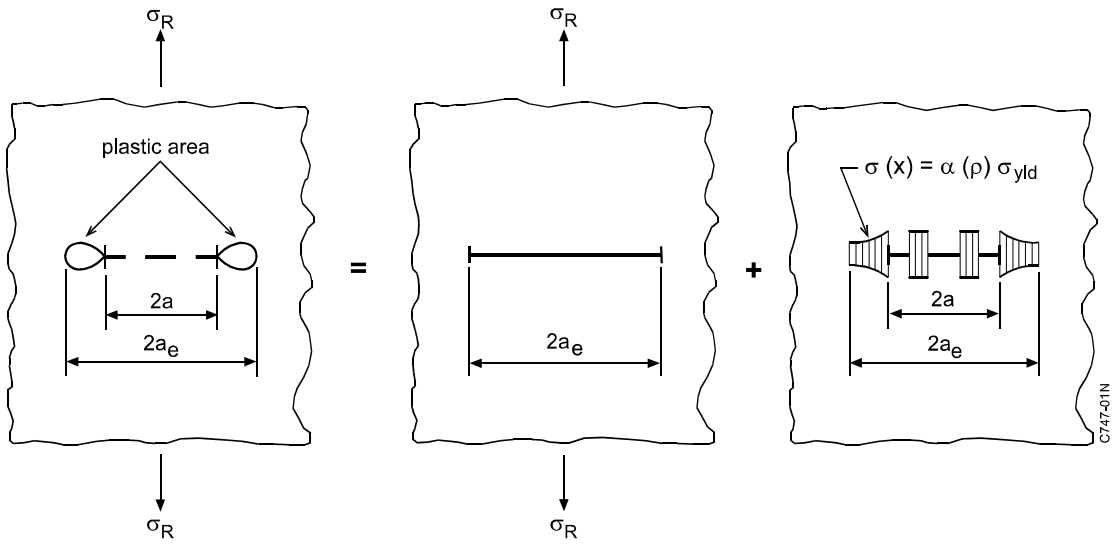

FIGURE 3. THE FICTITIOUS CRACK LENGTH ($2a_e$) AND LOAD CASES USED IN THE STRIP YIELD MODEL FOR MSD

3. RESIDUAL STRENGTH MODEL.

3.1 UNSTIFFENED PANELS.

The residual strength of a structure can be calculated by solving the following equations [12]:

$$G = R \tag{11}$$

$$\frac{\partial G}{\partial a} = \frac{\partial R}{\partial a} \tag{12}$$

where R is a material characteristic given in the form of a table or an expression, and G is obtained from the Strip Yield model. For simple geometries (like a center-cracked infinite sheet), there exists an explicit relation for G and R and for $\partial G/\partial a$ and $\partial R/\partial a$. In these cases, equations 11 and 12 can be solved directly. If the Strip Yield model is used to calculate G for multiple collinear cracks (MSD), there is no simple relation between G and a. The derivative of G with respect to a has to be solved numerically to be able to solve equations 11 and 12.

Alternatively, the following method can be used: Assume a remote load and calculated G for the initial crack length a_0. Solve the crack growth da_1 from equation 11. There is always a unique solution if the R-curve is monotonically increasing. The next step is to calculate G for a crack length $a_0 + da_{i-1}$ and solve a new da_i. This process is repeated until convergence has been obtained or until the failure criterion has been satisfied. If the assumed remote load is below the residual strength, this procedure will converge.

To solve the residual strength, an additional iterative procedure is required. If convergence has been obtained, the assumed remote load can be increased and the static growth can be solved again; if no convergence has been found, the assumed remote load should be decreased. With this in mind, an iterative procedure can be built to solve the residual strength (e.g., bisection method). This iterative procedure is probably not very efficient but it is suitable to solve the static growth of all tips. To do this, G and da have to be replaced by the vectors containing the energy release rates (as determined with the Strip Yield model) and static growth of all crack tips.

3.2 STIFFENED PANELS.

The effect of the stiffeners on the deformation behavior of a panel is implemented by the displacement compatibility method, as described by Vlieger [13] and Swift [14]. This method is based on the concept that displacements at all rivets in the cracked panel should be equal to the corresponding displacements in the stiffeners. This approach was first applied in ARREST, a computer program developed at NLR to predict the residual strength in stiffened panels with one crack.

Figure 4 shows a panel configuration with two riveted stiffeners and a single central crack of length 2a. The stiffener spacing is 2s. Each stiffener is fastened to the sheet by means of only one rivet at either side of the crack. The sheet is loaded at its ends by a uniform stress σ_R. Assuming equal displacements in the sheet and stiffener at the panel ends, this implies a stiffener end stress of $\sigma_R E_{st}/E_{sh}$, where E_{sh} and E_{st} are the Young's moduli of sheet and stiffener, respectively. Owing to the presence of the crack, the load will be transferred from the sheet to the stiffener via the rivets. To determine the displacements in the sheet and stiffener at the rivet locations due to the external stress σ_R and the interacting rivet forces F, the stiffened structure is split up into its components, as depicted in the central part of figure 4. The displacements in the sheet and the stiffener are denoted by v_{sh} and v_{st}, respectively. The displacement in the cracked sheet is composed of separate components, as indicated in the bottom part of figure 4, i.e., the displacement due to the remote stresses σ_R (v_a, see figure 4 (a)) and the displacement due to the rivet forces. The latter displacement is determined by considering this load case as a superposition of two load cases, i.e., the case of a sheet with rivet forces but no crack (displacement v_b, (see figure 4(b)) and that of a sheet with a crack loaded along its edges by a stress distribution $p(x)$ (displacement v_c, (see figure 4(c)). The stress distribution $p(x)$ is equal in magnitude, but of opposite in sign to the stresses along the crack segment caused by the rivet forces in the uncracked sheet of figure 4(b), and serves to provide the necessary stress-free crack surface. The displacements of the stiffener rivet points are composed of the displacements due to the end stress $\sigma_R E_{st}/E_{sh}$ and the displacements due to the rivet forces F. The rivet flexibility is

included by means of an empirical relation proposed by Swift [15]. Due to this rivet flexibility, there is a certain displacement of the rivets, v_{riv}, and the compatibility relation becomes

$$v_{sh} = v_{st} - v_{riv} \tag{13}$$

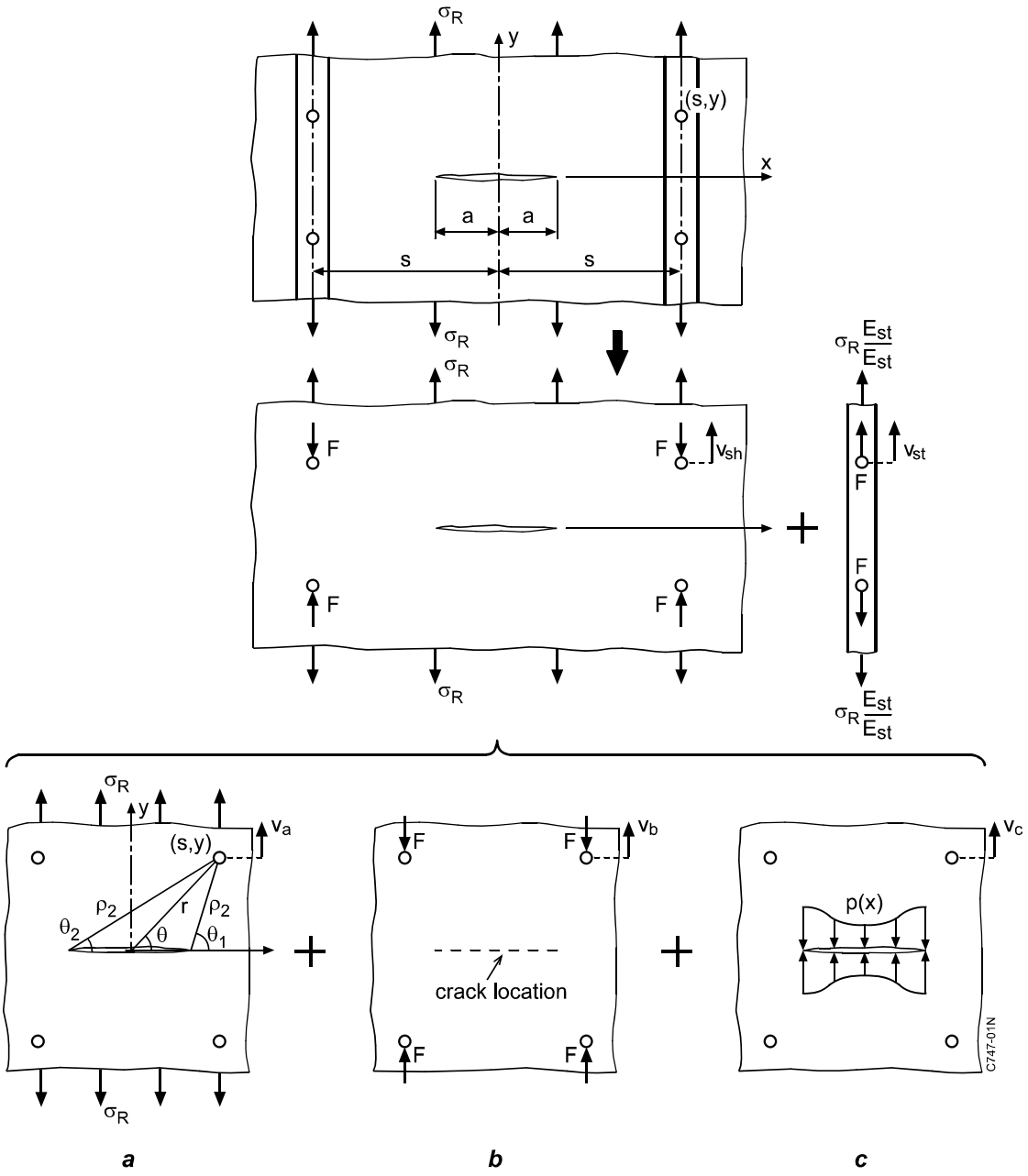

FIGURE 4. SPLIT UP OF CRACKED STIFFENED PANEL INTO ITS COMPONENTS

3.3 CURVED PANELS.

Longitudinal cracks in curved panels subjected to internal overpressure show in-plane and out-of-plane deformations of the crack faces. This so called bulging effect is caused by loss of hoop

tension reaction to the pressure loading [5 and 16] and in turn causes local bending at the crack tips, which increases the effective stress-intensity factor. In an engineering analysis, the stress-intensity factor for a curved panel can be calculated by multiplying the stress-intensity factor for a flat panel by an appropriate bulging factor (β_B). In this way, the same approach used to predict the residual strength for flat MSD panels could be applied once the bulging factor is known.

In the aerospace industry, the most frequently applied bulging factor comes from Swift [16]:

$$\beta_B = 1 + \frac{10a}{R} \tag{14}$$

where a is the half crack length and R the radius of curvature of the panel. It should be noted that this equation does not contain the internal pressure, which is known to have an effect on the bulging factor [17 and 18].

Chen and Schijve [17 and 18] investigated the bulging effect during the late eighties. They deduced a semiempirical equation, given by

$$\beta_B = \sqrt{1 + \frac{5}{3\pi}\frac{Eta}{R^2 p}\frac{0.316}{\sqrt{1+18\chi}}\tanh\left(0.06\frac{R}{t}\sqrt{\frac{pa}{Et}}\right)} \tag{15}$$

where E is the Young's modulus, t is the panel thickness, p is the internal pressure, and is χ is the biaxiality ratio (σ_x/σ_y, where y is the loading direction and x is the transverse direction). For an aluminium pressurized fuselage, which shows restrained lateral contraction, the biaxiality ratio obtained was $\chi = 0.24$.

Broek, et al. [5] deduced an expression for the bulging factor, based on R-curve data:

$$\beta_B = \sqrt{1 + \zeta\left[\left(\frac{E}{\sigma_0}\right)\left(\frac{a}{R}\right)^2\right]^{2/3}} \tag{16}$$

where σ_0 is the remote stress [1] and ζ is an empirical constant (0.671).

Figure 5 compares the three equations for the bulging factors as a function of the internal overpressure. The panel and crack geometry are similar to those described in Bigelow, et al. [19]. It is seen that the equation from Swift is the least suitable since it does not contain the internal pressure. The expression of Chen and Schijve results in a higher bulging factor than the expression of Broek, et al. Considering the thorough deduction of the Chen and Schijve expression (equation 15), its well-documented validation (by themselves, but also by Bigelow, et al. in reference 19), and the fact that the expression of Broek, et al. (equation 16) uses an empirical factor, ζ, which can be fitted to the experimental results, the Chen and Schijve

[1] For pressurised curved panels, the remote stress equals the hoop stress, which is given by pR/t, where p is the internal overpressure, R is the radius of curvature, and t is the sheet thickness

expression seems more reliable than that of Broek, et al. Moreover, some preliminary analyses on unstiffened curved Foster-Miller panels with one leading crack only, which made use of the bulging factor according to Broek, et al. (equation 16), showed very high failure stress, which might indicate a very small bulging factor. Therefore, all analyses on curved panels were done using the bulging factor according to Chen and Schijve. Figure 6 shows this bulging factor as a function of the internal pressure and the crack length, with panel and crack geometry similar to those used during the present analyses.

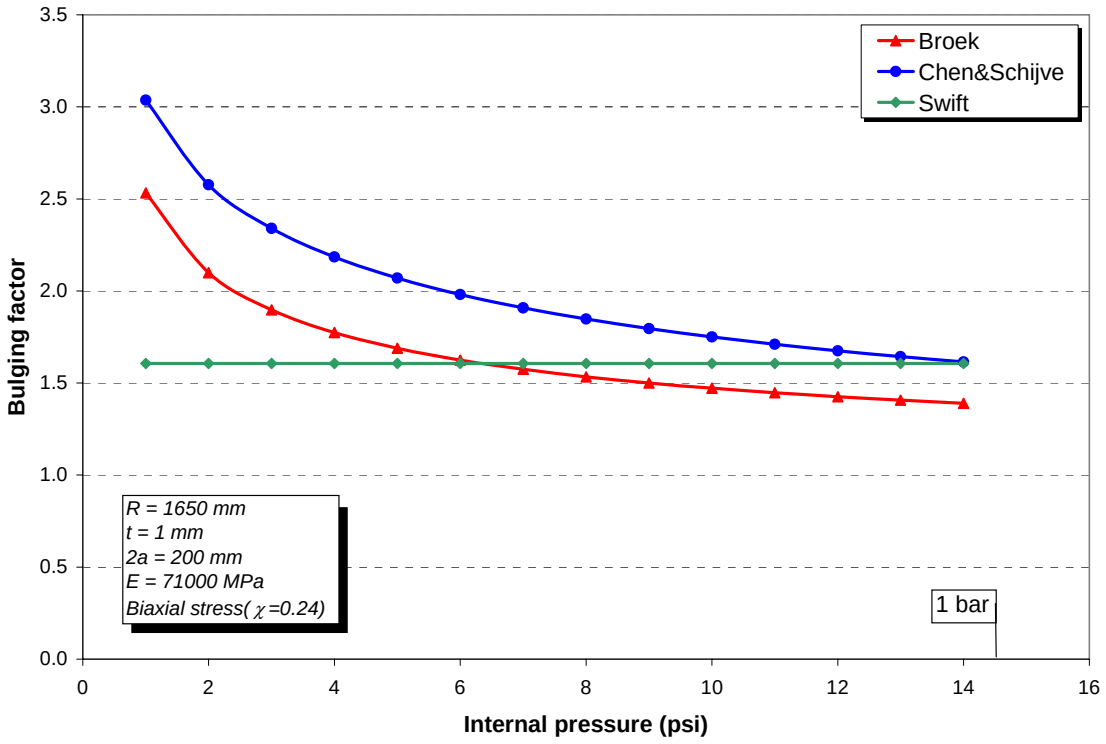

FIGURE 5. COMPARISON OF BULGING FACTOR ACCORDING TO SWIFT [16], CHEN AND SCHIJVE [17 AND 18], AND BROEK [5] AS A FUNCTION OF THE INTERNAL OVERPRESSURE AND FOR THE GIVEN GEOMETRY

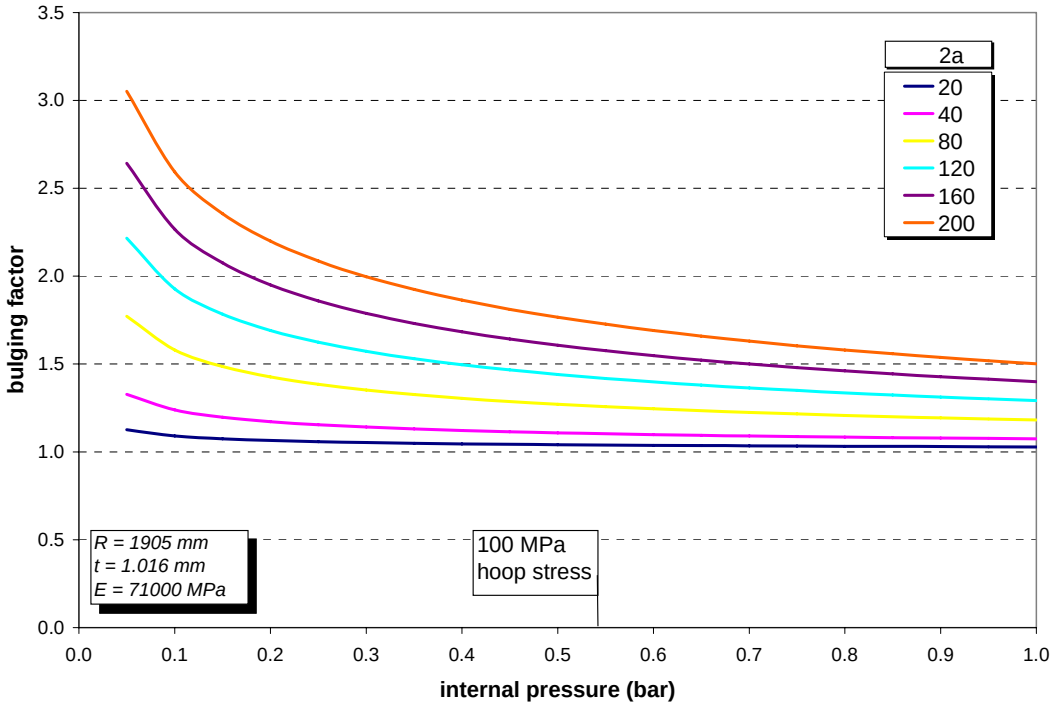

FIGURE 6. BULGING FACTOR ACCORDING TO CHEN AND SCHIJVE AS A FUNCTION OF THE INTERNAL (OVER) PRESSURE AND CRACK LENGTH AND FOR THE GIVEN GEOMETRY

For stiffened panels, however, the bulging effect is eliminated when the crack tip is in the vicinity of the stiffeners. Therefore, equation 15 is modified by using a damping factor. Swift [16] formulated this damping factor by assuming that maximum bulging occurs halfway between the stiffeners, that no bulging occurs at the stiffeners, and that the damping factor changes according to a cosine function between these two extremes. For a two-bay crack (i.e., crack extending under a stiffener), Swift proposed the following damping factor:

$$df = 0.5\left[1+\cos\left(\pi\left(1+\frac{2a}{L}\right)\right)\right] = 0.5\left[1-\cos\left(\frac{2\pi a}{L}\right)\right] \tag{17}$$

where a is the half crack length (i.e., the crack length at one side of the stiffener) and L is the frame spacing.

Based on Swift's considerations, Mor [20] suggested the following bulging factor for a symmetric one-bay crack (i.e., crack exactly between two stiffeners):

$$df = 0.5\left[1+\cos\left(\frac{2\pi a}{L}\right)\right] \tag{18}$$

However, MSD cracks are in general not exactly positioned between two stiffeners, which makes the damping factor no longer dependent on the crack length, as in equation 18, but on the distance from the crack tip to the nearest stiffener, *dL*. This yields the following expression:

$$df = 0.5\left[1-\cos\left(\frac{2\pi \cdot dL}{L}\right)\right] \tag{19}$$

When the crack tip is exactly midbay, then $dL = 0.5L$, the damping factor is $df = 1$, meaning maximum bulging. When the crack tip is at the stiffener, then $dL = 0$, the damping factor is $df = 0$, meaning no bulging. Substituting equation 19 in equation 15 gives

$$\beta_B = \sqrt{1+\frac{5}{3\pi}\frac{Eta}{R^2 p}\frac{0.316}{\sqrt{1+18\chi}}\tanh\left(0.06\frac{R}{t}\sqrt{\frac{pa}{Et}}\right)\cdot 0.5\left[1-\cos\left(\frac{2\pi \cdot dL}{L}\right)\right]} \tag{20}$$

It must be noted that the damping factor should actually be placed outside the square root of the bulging factor. However, the cosine shape of the damping factor is arbitrary, and in the literature, it is always placed under the square root [5, 16 through 18]. Be that as it may, it still varies between $df = 1$ and $df = 0$ for $dL = 0.5L$ and $dL = 0$, respectively. Since the residual strength is determined by the *J*-integral, which is a function of K^2, this means that *df* is in fact the damping factor for *J*.

3.4 LINKUP CRITERION.

As mentioned in section 1, models reported in the literature differ in definitions and criteria for crack growth and linkup. Swift [2] first proposed the linkup or plastic zone touch criterion. This criterion implies that a ligament will fail if the sum of the sizes of the two plastic zones of two crack tips equals the ligament size. This method has also been adopted by Broek, et al. [5] and De Wit, et al. [6], who determined the plastic zone with the Dugdale equation [9]. Broek, et al. [5] also applied a modified linkup criterion by including the effect of stable tearing, which reduces the distance between cracks and increases the stress-intensity factors. This modification increased the accuracy of the model predictions. Smith, et al. [7] modified the linkup model empirically to improve the accuracy of the model fit to the test data. Nilsson, et al. [8] defined linkup as actual crack impingement of the leading crack and an MSD crack. A two-parameter crack growth criterion based on a constant near-tip opening profile leads to crack growth resistance when used in conjunction with the Dugdale model. Onset of crack growth is determined by a critical crack opening, whereas continuous growth is governed by a constant crack opening angle.

The NLR model also defines linkup as the actual crack impingement of the leading crack and an MSD crack. However, as mentioned in section 3.1, the *R*-curve concept is used to assess the residual strength.

4. EXPERIMENTAL.

4.1 TEST DESCRIPTION.

The developed model was verified using experimental data from NLR, Foster-Miller, and the National Institute of Standards and Technology (NIST). All test panels were made from 2024-T3 aluminium without a lap joint. The NLR and Foster-Miller test panels were provided with an Alclad layer, while NIST used bare panels. NLR panels 4 to 14 (designed as NLR04 to NLR14) were stiffened with 7075-T6 strips, spaced every 340 mm. NLR04 to NLR09 consisted of a skin crack extending between two stiffeners, NLR10 consisted of a skin crack extending under an intact stiffener, and NLR11 to NLR14 consisted of a skin crack extending under a broken stiffener. The flat panels from Foster-Miller and NIST were unstiffened. Six of the nine Foster-Miller curved panels were stiffened with arrester straps (2024-T3 Alclad), whereby the lead crack extended under a broken central strap. Four of these panels (FMC4-7) were provided with light straps (width = 51 mm, height = 1 mm) and a small strap spacing (L = 254 mm). The other two panels (FMC8 and 9) were provided with heavy straps (width = 63.5 mm, height = 2 mm) and a doubled strap spacing (L = 508 mm).

Table 1 gives the geometry of the flat test panels and the MSD configuration, with parameters as defined in figure 7(a). The cracking patterns were symmetric with the same cracks at both sides of the hoop direction centerline. All secondary cracks were regularly distributed, which made it possible to describe the pattern by the parameters lig2, s_{MSD}, and $2a_{MSD}$. Table 2 gives the geometrical dimensions of the curved Foster-Miller panels and the MSD configuration, with parameters defined in figure 7(b). Again, the cracking patterns were symmetric, but the secondary cracks were not regularly distributed in some of the panels (FMC5, 6, 7, and 9). Therefore, figure 8 shows the cracking patterns in the curved stiffened panels.

TABLE 1. FLAT PANEL GEOMETRY AND MSD CRACK CONFIGURATION WITH PARAMETERS DEFINED IN FIGURE 7(a)

Test Panel	2W (mm)	t (mm)	H (m)	a_0 (mm)	d_{MSD} (mm)	$2a_{MSD}$ (mm)	lig1 (mm)	s_{MSD} (mm)	lig2 (mm)	No. Cracks per Side
NLR01	304	1.21	0.7	49.86	–	–	–	–	–	–
NLR02	304	1.21	0.7	50.03	69.45	13.20	12.82	–	–	1
NLR03	304	1.21	0.7	24.90	44.41	11.94	13.50	26.31	14.37	2
NLR04	1190	1.27	1.83	75.0	–	–	–	–	–	–
NLR05	1190	1.27	1.83	85.0	–	–	–	–	–	–
NLR06	1190	1.27	1.83	60.1	–	–	–	–	–	–
NLR07	1190	1.27	1.83	60.0	115.3	25.0	42.8	–	–	1
NLR08	1190	1.27	1.83	60.5	225.7	25.1	152.7	–	–	1
NLR09	1190	1.27	1.83	60.0	115.4	25.1	42.9	109.1	84.0	2
NLR10	1190	1.27	1.83	150.1	–	–	–	–	–	–
NLR11	1190	1.27	1.83	150.1	–	–	–	–	–	–
NLR12	1190	1.27	1.83	80.3	–	–	–	–	–	–
NLR13	1190	1.27	1.83	80.3	199.3	25.2	106.4	–	–	1

TABLE 1. FLAT PANEL GEOMETRY AND MSD CRACK CONFIGURATION WITH PARAMETERS DEFINED IN FIGURE 7(a) (Continued)

Test Panel	2W (mm)	t (mm)	H (m)	a_0 (mm)	d_{MSD} (mm)	$2a_{MSD}$ (mm)	lig1 (mm)	s_{MSD} (mm)	lig2 (mm)	No. Cracks per Side
NLR14	1190	1.27	1.83	80.0	176.6	25.1	84.1	118.2	93.1	2
FM01	508	1.016	1	50.8	–	–	–	–	–	–
FM02	508	1.016	1	88.9	–	–	–	–	–	–
FM03	508	1.016	1	134.2	–	–	–	–	–	–
FM04	508	1.016	1	76.2	114.3	12.7	31.8	–	–	1
FM05	508	1.016	1	91.4	114.3	12.7	16.6	–	–	1
FM06	508	1.016	1	96.5	114.3	12.7	11.5	38.1	25.4	2
FM07	508	1.016	1	94.0	114.3	12.7	14.0	38.1	25.4	3
FM08	508	1.016	1	101.6	114.3	7.6	8.9	25.4	17.8	2
FM09	508	1.016	1	40.7	63.5	20.3	12.6	50.8	30.5	2
FM10	508	1.016	1	40.7	63.5	12.7	16.5	38.1	25.4	2
FM11	508	1.016	1	63.5	88.9	25.4	12.7	50.8	25.4	2
FM12	508	1.016	1	38.1	88.9	25.4	38.1			1
NIST01	2286	1.016	3.988	177.8	–	–	–	–	–	–
NIST02	2286	1.016	3.988	101.6	–	–	–	–	–	–
NIST03	2286	1.016	3.988	254.0	–	–	–	–	–	–
NIST04	2286	1.016	3.988	177.8	190.5	10.2	7.6	25.4	15.2	3
NIST05	2286	1.016	3.988	71.1	88.9	15.2	10.2	38.1	22.9	3
NIST07	2286	1.016	3.988	254.0	266.7	12.7	6.3	38.1	25.4	5
NIST08	2286	1.016	3.988	241.3	266.7	12.7	19.1	38.1	25.4	10
NIST09	2286	1.016	3.988	127.0	165.1	10.2	33.0	25.4	15.2	10
NIST10	2286	1.016	3.988	254.0	266.7	12.7	6.3	38.1	25.4	5

NLR01 to NLR03, all FM, all NIST: Unstiffened
NLR04 to NLR09: Skin crack extending between two stiffeners
NLR10: Skin crack extending under an intact stiffener
NLR11 to NLR14: Skin crack extending under a broken stiffener

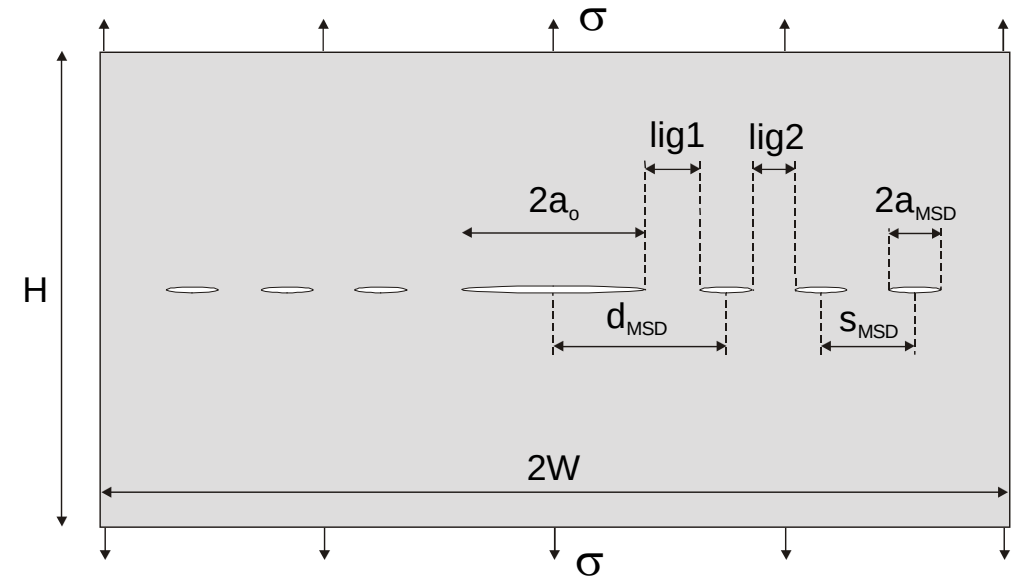

(a)

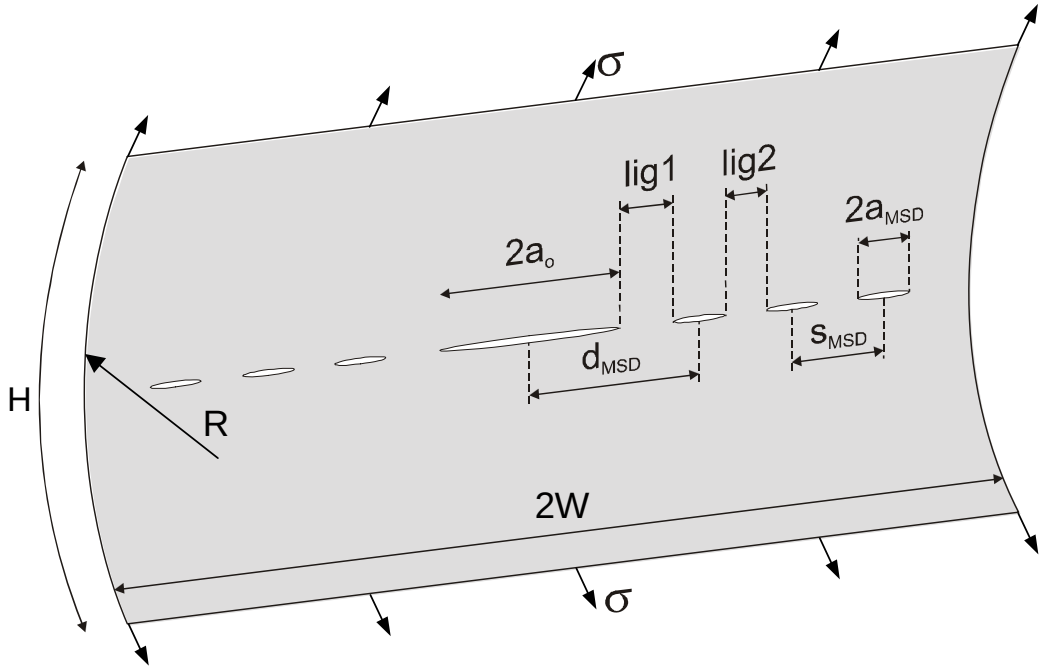

(b)

FIGURE 7. DESCRIPTION OF GEOMETRY PARAMETERS FOR (a) FLAT AND (b) CURVED MSD PANELS

TABLE 2. FOSTER-MILLER CURVED PANEL GEOMETRY AND MSD CRACK CONFIGURATION WITH PARAMETERS DEFINED IN FIGURE 7(b)

Test Panel	a_0 (mm)	d_{MSD} (mm)	$2a_{MSD}$ (mm)	lig1 (mm)	s_{MSD} (mm)	lig2 (mm)	No. Cracks per side
FMC1	139.7	–	–	–	–	–	–
FMC2	203.2	–	–	–	–	–	–
FMC3	139.7	177.8	50.8	12.7	101.6	50.8	2
FMC4	66.0	76.2	10.2	5.1	25.4	15.2	2
FMC5	66.0	76.2	10.2	5.1	[1]	[1]	10[1]
FMC6	106.7	127.0	10.2	15.2	[1]	[1]	6[1]
FMC7	147.3	203.2	10.2	50.8	[1]	[1]	4[1]
FMC8	88.9	101.6	10.2	7.6	25.4	15.2	3
FMC9	109.2	127.0	10.2	12.7	[1]	[1]	12[1]

2W= 3048 mm
t= 1.016 mm
H= 1.73 m
R= 1905 mm
[1] small cracks are on irregular mutual distance

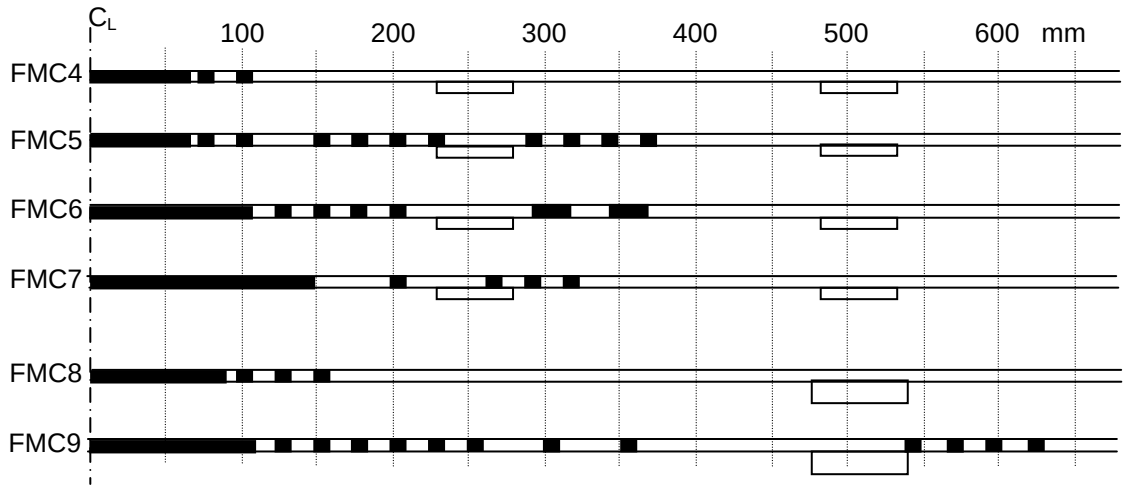

FIGURE 8. CRACK CONFIGURATIONS OF CURVED MSD PANELS FROM FOSTER-MILLER TESTS

The tests on the flat panels were conducted under displacement control. These panels were fabricated with antibuckling guides to avoid out-of-plane deflection. The curved panels were loaded by internal pressurization. More details of the tests can be found in references 3 and 4 for the NLR tests (except for the first three tests, which are not described in the open literature), references 1 and 5 for the Foster-Miller tests, and reference 6 for the NIST tests.

4.2 *R*-CURVE.

The *R*-curve used for all model predictions was derived from the a-N data of the NLR04 test panel. It was not determined according to American Society for Testing and Materials (ASTM) E 561-86, but from the model itself, by calculating the corresponding point on the *G*-curve for each stress step. In this way, an *R*-curve is obtained including all model features and assumptions involved. Figure 9 shows the *R*-curve used during the present analyses in comparison with the *R*-curve determined from the same a-N data, but now according to ASTM E 561-86 and with the *R*-curve used for the Foster-Miller panel analyses [5].

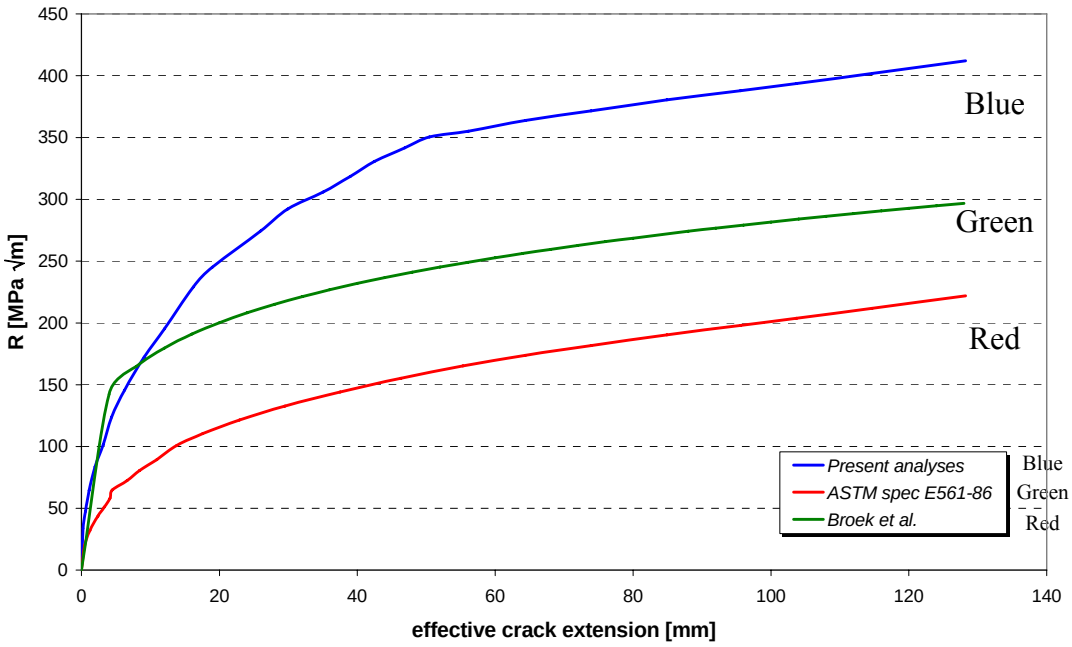

FIGURE 9. *R*-CURVE USED DURING THE PRESENT ANALYSES IN COMPARISON WITH THE *R*-CURVE DETERMINED FROM THE SAME a-N DATA, BUT ACCORDING TO ASTM E 561-86 AND WITH THE *R*-CURVE USED BY BROEK, ET AL. FOR THE FOSTER-MILLER PANEL ANALYSES [5]

4.3 FLOW STRESS.

All predictions were made with the flow stress, σ_Y, instead of the yield strength, σ_{YS}. The flow stress is the average between the yield strength and the ultimate tensile strength (UTS):

$$\sigma_Y = (\sigma_{YS} + UTS)/2 \tag{21}$$

This was done because the model assumes linear elastic/ideal plastic material behavior while 2024-T3 manifests strain hardening. Previous experiments at the NLR [4] showed that equation 21 results in $\sigma_Y = 424$ MPa. This value seemed too high for 2024-T3. However, it was obtained from the same batch of material used for the *R*-curve test, so it was adopted for all analyses.

5. RESULTS AND DISCUSSION.

5.1 CALCULATION TIME.

The calculation times depended strongly on the panel and MSD configuration. The flat panel calculations were done on a Pentium III with a 733-MHz processor. The calculation times varied from only a few seconds for an unstiffened panel with a leading crack to 16 minutes for an unstiffened panel with 10 secondary cracks on both sides of a leading crack (NIST09), and 14 minutes for a stiffened panel with two secondary cracks on both sides of a leading crack (NLR09). The curved panel calculations were done with an Athlon XP 2200+ processor. The calculation times varied from only a few seconds for an unstiffened panel with a leading crack to 200 minutes for a curved panel with 13 secondary cracks on both sides of a leading crack (FMC9).

5.2 LINKUP AND RESIDUAL STRENGTH.

Table 3 and figures 10 through 12 give the comparisons between model prediction and experimental results from the NLR, Foster-Miller, and NIST tests on flat panels. There is fair agreement between the predicted values and the experimental values, especially for the linkup stresses. It was, however, observed that the prediction for the failure stress is in many cases too high, both for a flat panel with a leading crack only (NLR01, 04, 10-12; FMF01-03; NIST01-03) and for a flat panel with MSD cracks (i.e., final failure after linkup). The reason for this can be found in the application of the *R*-curve approach. Since the *R*-curve is based on a residual strength experiment with a panel of limited width (NLR04), the *R*-curve becomes unreliable for large crack lengths just before failure.

TABLE 3. COMPARISON OF TEST DATA AND ANALYTICAL PREDICTIONS FOR STRESS (MPa) AT FIRST AND SECOND LINKUP AND AT FINAL FAILURE IN FLAT PANELS

Panel	Final Failure			1st Linkup			2nd Linkup		
	Test	Model	Δ (%)	Test	Model	Δ (%)	Test	Model	Δ (%)
NLR01	206	229	11						
NLR02	150	172	15	134	132	-1			
NLR03	174	173	-1	174	185	6	174	176	1
NLR04	297	317	7						
NLR05	297	285	-4						
NLR06	297	285	-4						
NLR07	244	277	14	207	186	-10			
NLR08	276	275	0	276	275	0			
NLR09	246	261	6	205	186	-9	257	261	2
NLR10	195	260	33						
NLR11	179	181	1						
NLR12	183	199	9						
NLR13	179	198	11	174	181	4			
NLR14	177	191	8	169	169	0	147	160	9

TABLE 3. COMPARISON OF TEST DATA AND ANALYTICAL PREDICTIONS FOR STRESS (MPa) AT FIRST AND SECOND LINKUP AND AT FINAL FAILURE IN FLAT PANELS (Continued)

Panel	Final Failure			1st Linkup			2nd Linkup		
	Test	Model	Δ (%)	Test	Model	Δ (%)	Test	Model	Δ (%)
FMF01	214	250	17						
FMF02	163	190	17						
FMF03	114	140	23						
FMF04	155	171	10	155	171	10			
FMF05	130	161	24	119	121	1			
FMF06	111	121	9	100	91	-9	111	111	0
FMF07	110	93	-16	110	101	-9	110	111	1
FMF08	111	131	18	97	91	-7	110	111	1
FMF09	152	151	-1	145	131	-10	152	151	-1
FMF10	172	171	0	172	171	-1	172	161	-6
FMF11	110	121	10	106	101	-5	110	111	1
FMF12	195	210	8	195	210	8			
NIST01	147	170	16						
NIST02	184	210	14						
NIST03	124	150	21						
NIST04	132	151.9	15	84	60.6	-28	98	81.3	-17
NIST05	175	171.9	-2	138	100.6	-27	161	141.3	-12
NIST07	148	116.6	-21	56	45.3	-19	171	90.6	-47
NIST08	73	86.3	18	89	80.6	-9	91	91.2	0
NIST09	119	116.3	-2	152	140.6	-8			
NIST10	100	116.6	17	66	45.3	-31	95	90.6	-5

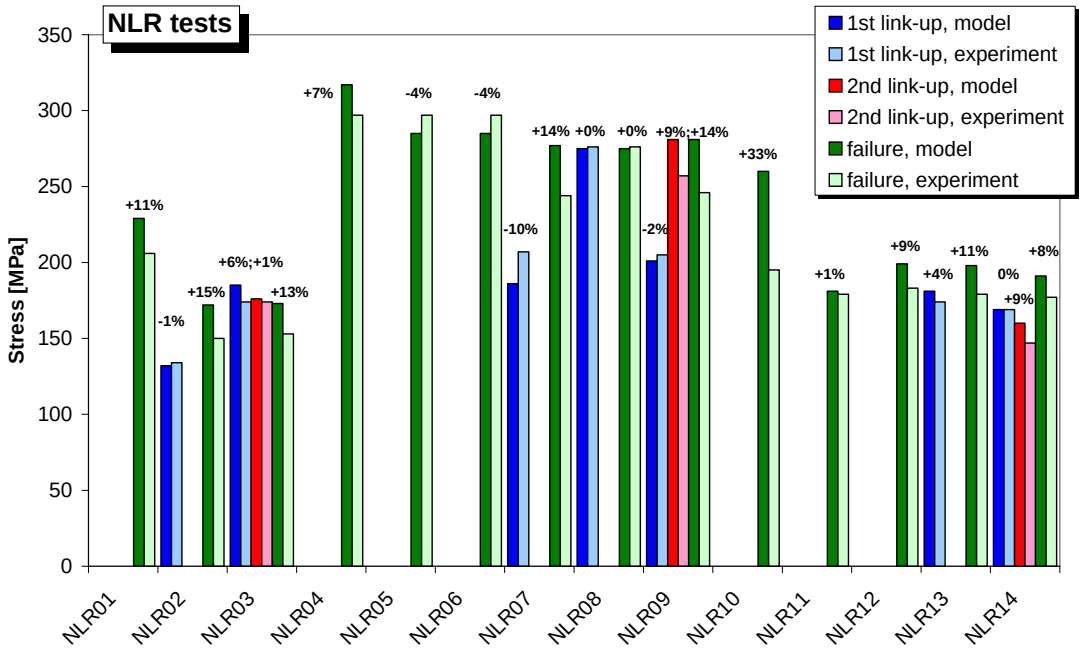

FIGURE 10. PREDICTED AND MEASURED STRESS LEVELS FOR LINKUP AND FAILURE FOR THE NLR MSD PANELS
(The relative deviation of the predictions from the experimental values is given at the top of each bar.)

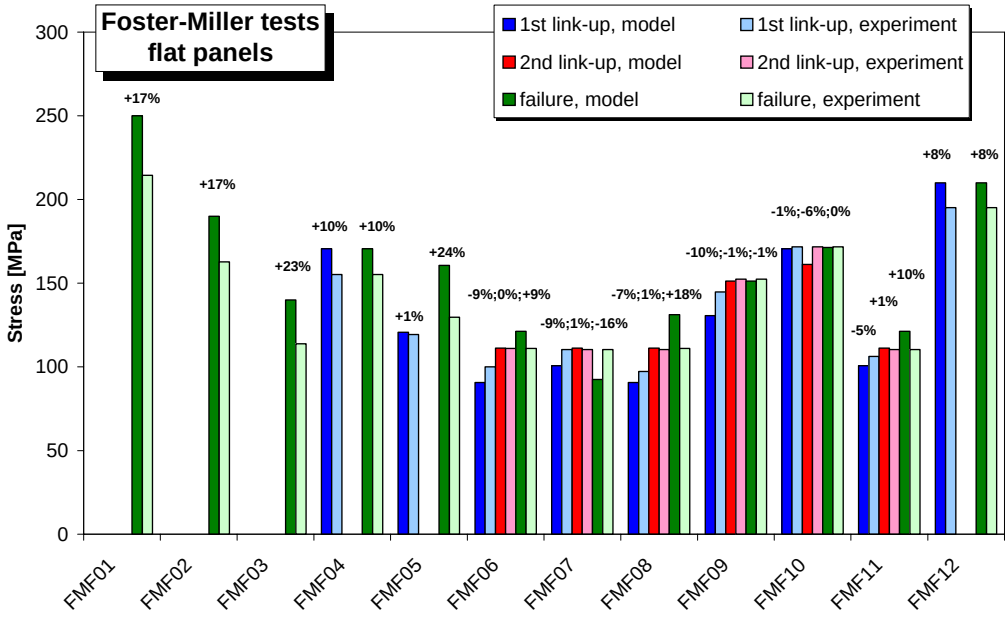

FIGURE 11. PREDICTED AND MEASURED STRESS LEVELS FOR LINKUP AND FAILURE FOR THE FOSTER-MILLER FLAT MSD PANELS
(The relative deviation of the predictions from the experimental values is given at the top of each bar.)

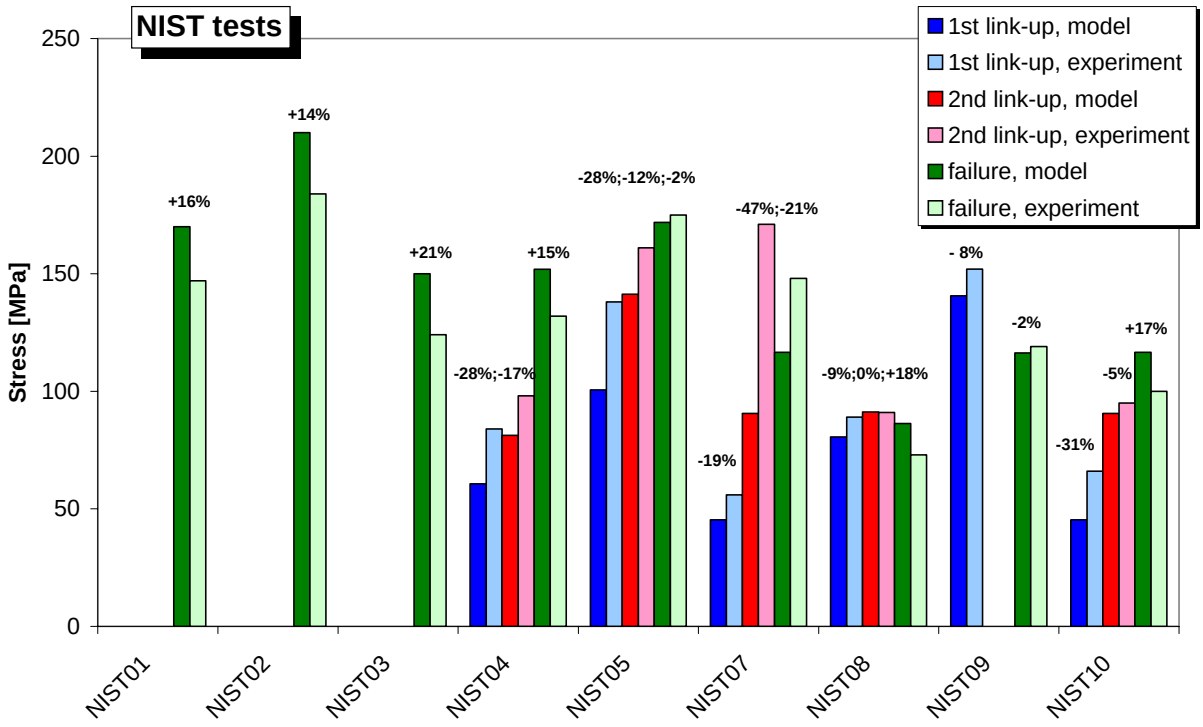

FIGURE 12. PREDICTED AND MEASURED STRESS LEVELS FOR LINKUP AND FAILURE FOR THE NIST MSD PANELS
(The relative deviation of the predictions from the experimental values is given at the top of each bar.)

Table 4 and figure 13 give the comparisons between model prediction and experimental results from the Foster-Miller tests for curved panels. For a curved panel with a leading crack only (FMC1 and 2), the prediction for the failure stress is good, or even too low. This indicates that the used bulging factor probably overestimated the bulging effect, since for the flat panels with a leading crack only, the predicted failure stress was too high (see above). However, as mentioned in section 3.3, the predictions obtained with this bulging factor (from Chen and Schijve) were better than those with the bulging factor according to Broek, et al. The prediction for the failure stress for the stiffened panels with MSD cracks was in general very high (FMC4, 6, 7, and 8). This might be contributed to the location of the stiffeners. For these panels, the crack extended to the stiffener before final failure. This means that the failure of the stiffener was calculated with an *R*-curve that was not reliable. For the linkup stresses, there is, again, good agreement between the predicted and experimental values.

TABLE 4. COMPARISON OF TEST DATA AND ANALYTICAL PREDICTIONS FOR STRESS (MPa) AT FIRST AND SECOND LINKUP AND AT FINAL FAILURE IN CURVED FOSTER-MILLER PANELS

Panel	Final Failure			1st Linkup			2nd Linkup		
	Test	Model	Δ (%)	Test	Model	Δ (%)	Test	Model	Δ (%)
FMC1	84	83	-1						
FMC2	63	52	-18						
FMC3	54	36	-34	32	36	11	54	36	-34
FMC4	152	246	61	78	55	-29	105	96	-8
FMC5	124	126	2	78	55	-29	105	96	-8
FMC6	117	182	56	77	80	5	77	80	5
FMC7	117	165	42	103	130	26	117	130	12
FMC8	92	181	97	75	50	-34	81	61	-25
FMC9	68	55	-19	68	55	-19	68	55	-19

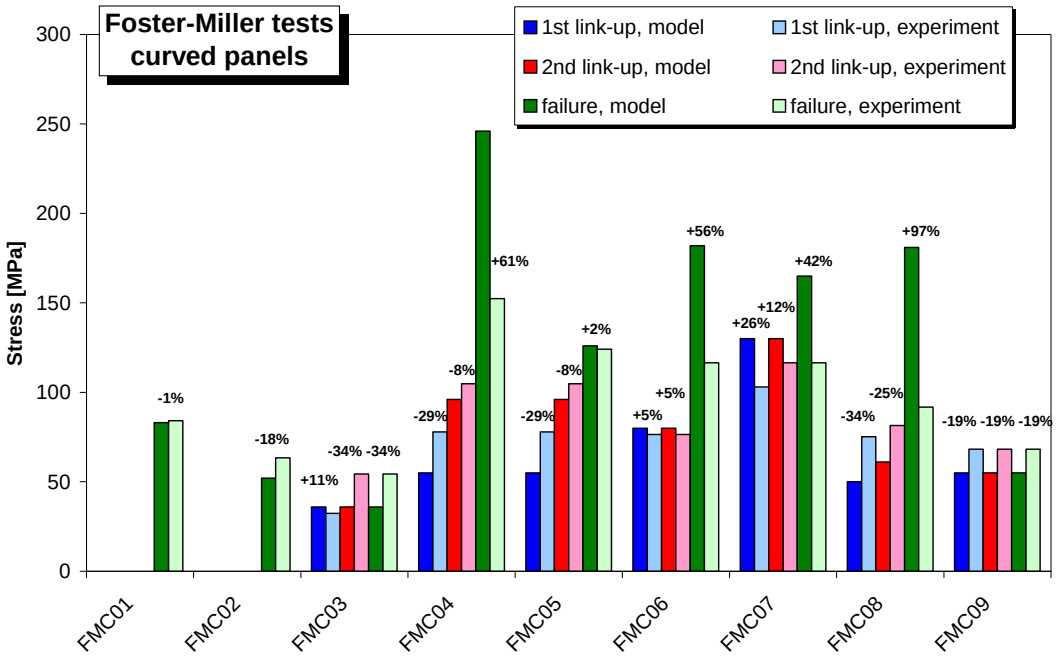

FIGURE 13. PREDICTED AND MEASURED STRESS LEVELS FOR LINKUP AND FAILURE FOR THE FOSTER-MILLER CURVED MSD PANELS
(The relative deviation of the predictions from the experimental values is given at the top of each bar.)

5.3 CRACK GROWTH.

During the NLR tests, static crack growth was observed in all panels. Crack length data were obtained as a function of the applied load. This enabled verification of the entire crack growth and linkup process predicted by the model. The experimental results are reported by Ten Hoeve,

et al. [4]. Figures 14 to 18 shows five representative examples of unstiffened and stiffened panels (NLR01, NLR03, NLR09, NLR13, and NLR14).

The crack growth process was predicted fairly well, especially during the linkup phase. Crack growth just before failure deviated from the measured values of the application of the *R*-curve approach.

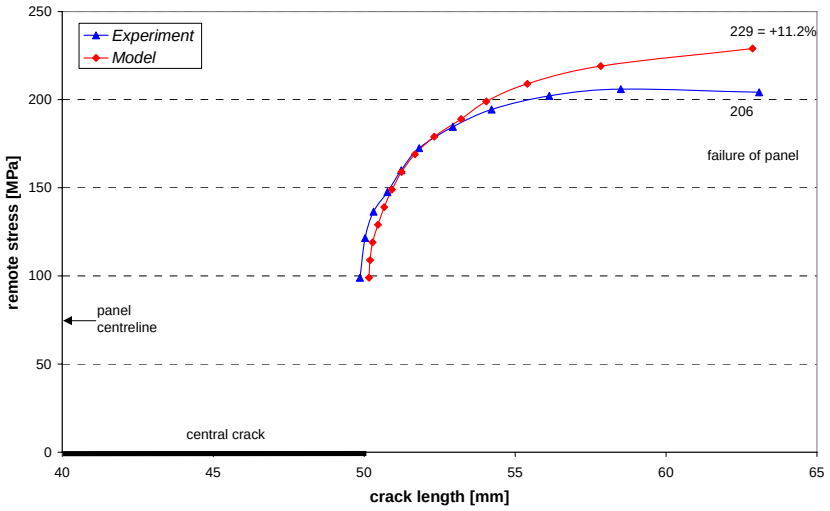

FIGURE 14. PREDICTED AND MEASURED CRACK GROWTH AS A FUNCTION OF THE APPLIED REMOTE STRESS FOR THE NLR01 PANEL
(The relative deviations of the predictions from the experimental values are indicated.)

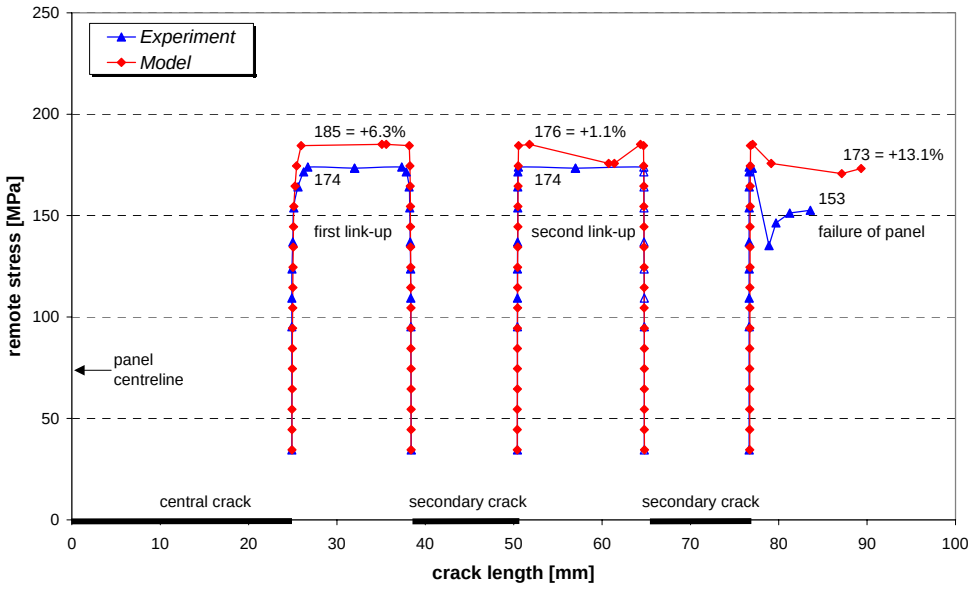

FIGURE 15. PREDICTED AND MEASURED CRACK GROWTH AS A FUNCTION OF THE APPLIED REMOTE STRESS FOR THE NLR03 PANEL
(The relative deviations of the predictions from the experimental values are indicated.)

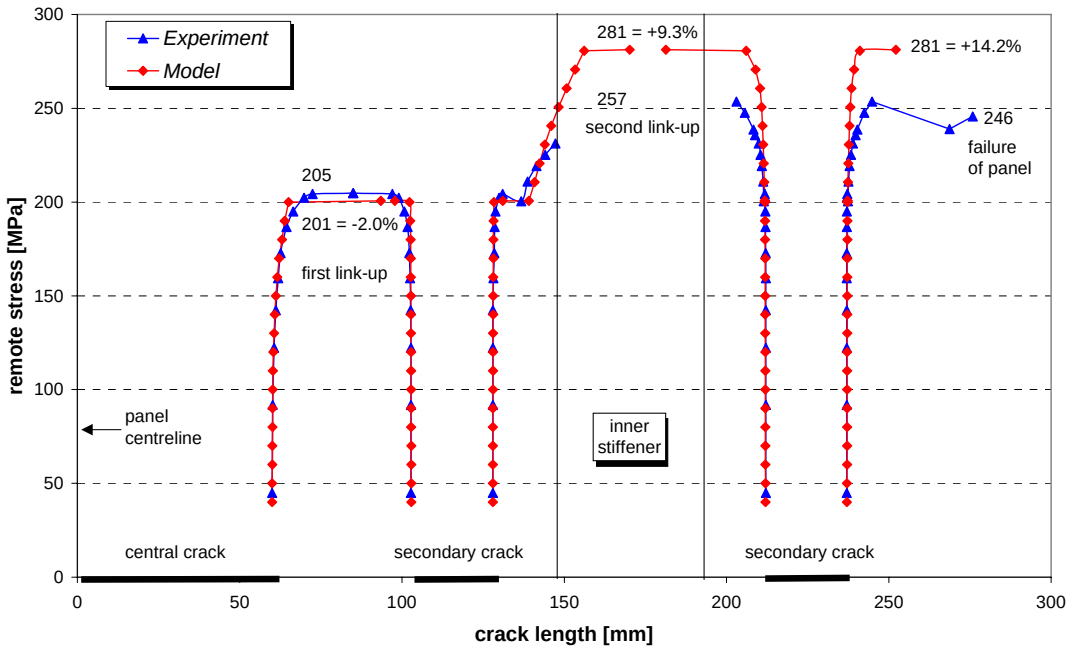

FIGURE 16. PREDICTED AND MEASURED CRACK GROWTH AS A FUNCTION OF THE APPLIED REMOTE STRESS FOR THE NLR09 PANEL
(The relative deviations of the predictions from the experimental values are indicated.)

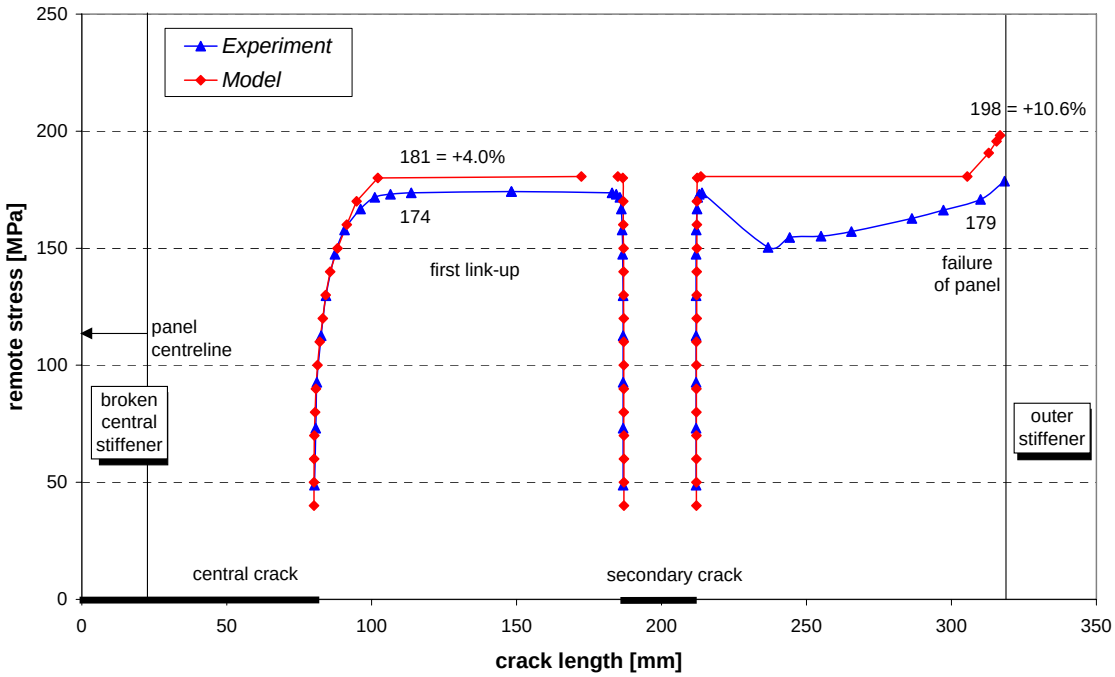

FIGURE 17. PREDICTED AND MEASURED CRACK GROWTH AS A FUNCTION OF THE APPLIED REMOTE STRESS FOR THE NLR13 PANEL
(The relative deviations of the predictions from the experimental values are indicated.)

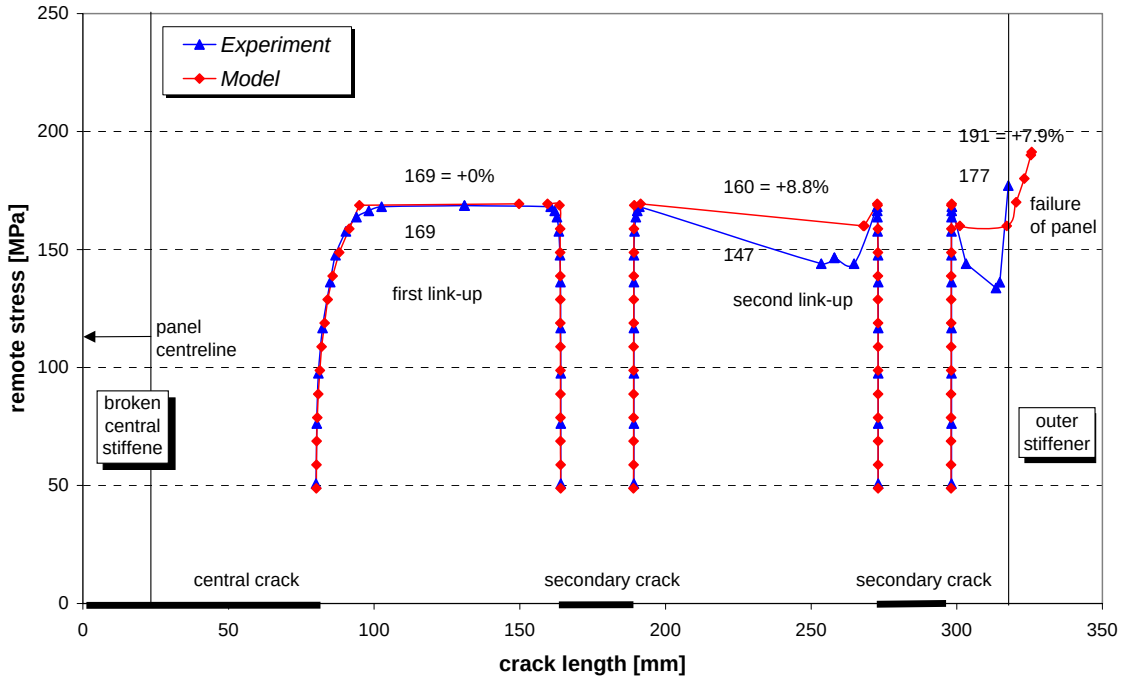

FIGURE 18. PREDICTED AND MEASURED CRACK GROWTH AS A FUNCTION OF THE APPLIED REMOTE STRESS FOR THE NLR14 PANEL
(The relative deviations of the predictions from the experimental values are indicated.)

6. SUMMARY.

An advanced engineering model to predict linkup and residual strength in flat and curved unstiffened and stiffened panels with one leading crack and MSD cracks was presented. This model was based on the Strip Yield model for calculation of the *J*-integral at all crack tips and the *R*-curve approach. The influence of stiffeners was modeled using the displacement compatibility method. The effect of panel curvature was incorporated with bulging factor, and linkup was defined as actual crack impingement.

After model verification with experimental results from different institutes, it was observed that the predicted failure stress was generally very high for the application of the *R*-curve concept. For the linkup stresses, there was fair agreement between the predicted and the experimental values, but no general trends in the deviation between the model and experiment could be observed. This makes it difficult to explain the differences from a modeling point of view. One should consider the possibility of inaccuracies in the experimental results, since for all but one test there were no duplicates. The only duplicate tests carried out were NIST07 and NIST10 panels. The differences between these two tests on identical panels are rather large: 18% for first linkup, 44% for second linkup, and 32% for panel failure. Hence, the observed deviation of the predictions from the experimental results lie within the experimental variation. Also, the observed deviations are similar to those found by Broek, et al. [5], De Wit, et al. [6], and Nilsson [8]. Smith, et al. [7] obtained somewhat better predictions, but after fitting their model to the experimental results, i.e., semiempirical model was used. It should be noted that a better

validation of the model would require more duplicate tests with the same MSD configuration, i.e., a statistically more reliable experimental result.

7. CONCLUSIONS.

From the model verification presented in this report, the following conclusions were drawn:

- The predicted linkup loads and residual strengths agreed fairly well with the experimental values.
- The observed deviations for the linkup stresses fell within the experimental errors reported in the literature. However, more duplicate tests are recommended to obtain statistically reliable test results.
- The *R*-curve approach in combination with actual crack impingement as linkup criterion resulted in good predictions for the linkup stresses and the crack growth during the linkup phase.
- The predictions for residual strength and crack growth just before failure were generally higher than the measured values, owing to the unreliability of the *R*-curve for long cracks. The *R*-curve should actually be based on a wider panel.
- The bulging factor according to Chen and Schijve seemed to account well for the bulging effect due to panel curvature.

8. REFERENCES.

1. Schijve, J., "Multiple-Site Damage in Aircraft Fuselage Structures," *Fatigue Fract. Engng. Mater. Struct.*, Vol. 18, 1995, pp. 329-344.
2. Swift, T., "Widespread Fatigue Damage Monitoring – Issues and Concerns," in *Proc. 5th Int. Conf. on Structural Airworthiness of New and Aging Aircraft*, 1993, pp. 113-150.
3. Hoeve, ten, H.J., Ottens, H.H., Schra, L., and Vlieger, H., "Residual Strength of Stiffened Panels With Multiple-site damage," in *Proc. 7th Int. Fatigue Congress*, X.R. Wu and Z.G. Wang, eds., Vol. 4, Higher Education Press, Beijing, China, 1999, pp. 2515-2520.
4. Hoeve, ten, H.J., Schra, L., Michielsen, A.L.P.J., and Vlieger, H., "Residual Strength Tests on Stiffened Panels With Multiple-site damage," NLR-CR-96792 L, National Aerospace Laboratory, Amsterdam, The Netherlands, 1996.
5. Broek, D., Jeong, D.Y., and Thomson, D., "Testing and Analysis of Flat and Curved Panels With Multiple Cracks," in *Proc. FAA/NASA Int. Symp. Advanced Structural Integrity Methods for Airframe Durability and Damage Tolerance*, NASA Conference Publication 3274, 1994, pp. 85-98.

6. De Wit, R., Fields, R.J., Low III, S.R., Harne, D.E., and Foecke, T., "Fracture Testing of Large Scale Thin-Sheet Aluminum Alloy," National Inst. of Standards and Technology, NISTIR 5661, Gaithersburg, MD, USA, 1995.

7. Smith, B.L., Saville, P.A., Mouak, A., and Myose, R.Y., "Strength of 2024-T3 Aluminum Panels with Multiple-site damage," *Journal of Aircraft*, Vol. 37, No. 2, 2000, pp. 325-331.

8. Nilsson, K.F., "Elasto-Plastic Models for Interaction Between a Major Crack and Multiple Small Cracks," in *Proc. FAA/NASA Symposium on Continued Airworthiness of Aircraft Structures*, Atlanta, GA, 1996.

9. Dugdale, D.S., "Yielding of Steel Plates Containing Slits," *Journal of the Mechanics and Physics of Solids*, Vol. 8, 1960, pp. 100-108.

10. Tada, H., Paris, P.C., and Irwin, G.R., "The Stress Analysis of Cracks Handbook", Del Research Corporation, St. Louis, MO, USA, 1973.

11. Brice, J.R., "Plastic Yielding at a Crack Tip," in *Proc. First Int. Conf. on Fracture*, Vol. 1, T. Yokobori, T. Kawasaki, and J.L. Swedlow, eds., The Japanese Society for Strength and Fracture of Materials, 1966, pp. 283-308.

12. Ewalds, H.L. and Wanhill, R.J.H., "Fracture Mechanics", Edward Arnold Ltd, London, UK/Delftse Uitgevers Maatschappij b.v., Delft, The Netherlands, 1984.

13. Vlieger, H. and Sanderse, A., "User's Manual of Arrest, a Computer Routine for Prediction of Residual Strength of Cracked Stiffened Panels," NLR TR 75129 C, National Aerospace Laboratory NLR, Amsterdam, The Netherlands, 1975.

14. Swift, T., "Fracture Analysis of Stiffened Structure," Damage Tolerance of Metallic Structures: Analysis Methods and Applications, ASTM STP 842, J.B. Chang and J.L. Rudd, eds., American Society for Testing and Materials, 1984, pp. 69-107.

15. Swift, T., "Development of the Fail-Safe Design Features of the DC-10," Damage Tolerance in Aircraft Structures, ASTM STP 486, ASTM, Philadelphia, PA, USA, 1971, pp. 164-214.

16. Swift, T., "Design of Redundant Structures," in *Fracture Mechanics Design Methodology*, AGARD-LS-97, North Atlantic Treaty Organization, London, England, 1979, pp. 9.1-9.23.

17. Chen, D., "Bulging of Fatigue Cracks in a Pressurized Aircraft Fuselage," PhD-thesis, Delft University of Technology, Faculty of Aerospace Engineering, Report LR-647, October 1990.

18. Chen, D. and Schijve, J., "Bulging of Fatigue Cracks in a Pressurized Aircraft Fuselage," Delft University of Technology, Faculty of Aerospace Engineering, Report LR-655, May 1991. Presented at *16th ICAF Symposium*, Tokyo, Japan, 22-24 May 1991.

19. Bigelow, C.A., Bakuckas, J.G. Jr., Tan, P.W., Lee, X., and Rahman, A., "Crack Bulging Effects in Longitudinal Cracks in Pressurized Narrow Body Aircraft," Presented at *21st ICAF Symposium*, Toulouse, France, 27-29 June 2001.

20. Mor, H., "Crack Propagation Analysis of Longitudinal Skin Cracks in a Pressurized Cabin," in *Proc. 26th Israel Annual Conference on Aviation and Astronautics*, Tel Aviv, Israel, 1984, pp. 78-83.